DOI 10.1007/s10812-022-01438-x
Journal of Applied Spectroscopy, Vol. 89, No. 5, November, 2022 (Russian Original Vol. 89, No. 5, September–October, 2022)

CRYSTAL STRUCTURE AND ELECTRONIC PROPERTIES OF RHENIUM DISULFIDE**

A. V. Baglov[a,b,*] and L. S. Khoroshko[a,b]

UDC 544.225.22/.23+544.183.24/.25:538.911+538.915

The crystal structure and electronic properties of rhenium disulfide in the triclinic crystal system are investigated using density functional theory and pseudopotential theory. The calculated primitive cell parameters and angles within a local density approximation are shown to be in good agreement with the experimental data. It is established that the observed direct-gap character of rhenium disulfide is related to interband transitions at point X. The electron energy spectrum is characterized by many valleys. The electronic structure is mainly formed by the 3p- and 5d-states of sulfur and rhenium ions, respectively. The role of 5d-states increases while that of 3p-states decreases during the transition from the valence band to the conductance band. The observed structure is due to the low symmetry of the primitive cell and the numerous nonequivalent positions of its constituent ions.

Keywords: *dichalcogenides, disulfides, rhenium, rhenium disulfide, density functional theory, pseudopotential theory, electronic structure, density of states.*

Introduction. Transition-metal dichalcogenides (TMDs) attract the attention of researchers because of the unique combination of a layered structure and electronic properties that make them promising in various sectors. Disulfides of molybdenum (MoS_2) and tungsten (WS_2) are TMDs that have been extensively studied as catalysts for hydrogen production via electrochemical decomposition of H_2O [1, 2], as components for lithium-ion battery anodes [3], as materials for gas sensors [4], as subnanometer transistors for next-generation electronics [5], etc.

Rhenium disulfide (ReS_2) has been studied much less although published experimental work allows the material to be characterized as promising. Nanostructured ReS_2 has been used as a (photo)catalyst [6, 7] and to form vertically oriented arrays of nanosheets by chemical vapor deposition that showed potential for creating lithium–sulfur batteries with very small capacity losses in charge/discharge cycles [8]. This material was also used as thin films to construct a high-sensitivity detector of polarized light [9] and a phototransistor [10]. The possibility of using ReS_2 to fabricate field transistors was interesting [11]. The properties of ReS_2 and its possible practical applications have been thoroughly reviewed [12]. To the best of our knowledge, new reviews on this material have not been published.

The structures of Re, Mo, and W disulfides differ considerably, despite them being layered materials. Crystals of ReS_2 belong to the triclinic system [13]; MoS_2 and WS_2, hexagonal [14, 15]. The distortion inherent in the low-symmetry ReS_2 unit cell makes it a potential material for establishing an elemental basis of straintronics. The ability to replace sulfur ions by other chalcogenide ions enables the synthesis of solid solutions of ternary Re chalcogenides with variable physicochemical properties over a relatively wide range. However, the role of Re and S ions in formation of the electronic structure has not been systematically investigated. Also, the structural properties have not been described by quantum-mechanical modeling.

The goal of the present work was to evaluate the applicability of a quantum-mechanical approach to the study of the crystal structure of triclinic ReS_2 and to analyze its electronic properties in terms of *ab initio* methods.

Experimental. Numerical modeling in terms of density functional theory and pseudopotential theory was performed using OpenMX software [16–18]. The starting unit cell was constructed using experimental data [13]. The convergence criterion for the self-consistent field calculation was 10^{-6} eV/ion. The first Brillouin zone was integrated over a Γ-centered

*To whom correspondence should be addressed.

**Presented at the X International School-Conference of Young Scientists and Specialists, Current Problems of Physics-2022, B. I. Stepanov Institute of Physics, National Academy of Sciences of Belarus, April 27–29, 2022, Minsk, Belarus.

[a]Belarusian State University, Minsk, Belarus; email: baglov@bsu.by; [b]Belarusian State University of Informatics and Radioelectronics, Minsk, Belarus. Translated from Zhurnal Prikladnoi Spektroskopii, Vol. 89, No. 5, pp. 651–656, September–October, 2022. Original article submitted August 12, 2022; https://doi.org/10.47612/0514-7506-2022-89-5-651-656.

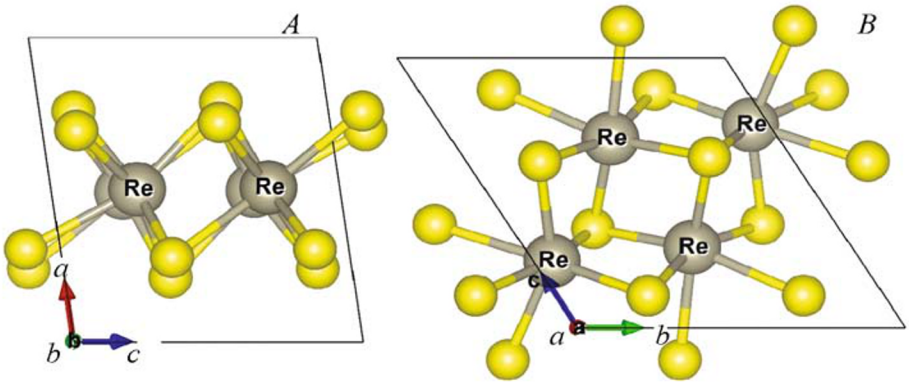

Fig. 1. Unit cell of ReS_2: view from the side (*A*) and above (*B*).

regular grid of *k*-points of dimension 4 × 5 × 5. The grid for numerical integration had dimension 46 × 39 × 40 points, which corresponded approximately to the mean cut-off energy of 2100 eV. Pseudopotentials included 5*s*, 5*p*, 5*d*, and 6*s* valence electrons for Re and 3*s* and 3*p* electrons for S. The basis set was built as a linear combination of pseudoatomic orbitals using two optimized basis functions for each valence electron with one additional optimized basis function as polarization for a more accurate consideration of chemical bonding in the crystal and correct reproduction of energy band dispersion. Numerical modeling was performed in terms of a local density approximation and exchange-correlated Ceperley–Alder functional [19]. These parameters were chosen because the structural properties of layered materials could be correctly described with a distinct van der Waals interaction between layers, including in MoS_2 and WS_2 [20, 21]. The density of electronic states was calculated using the method of tetrahedra over a Γ-centered regular grid of *k*-points of dimension 5 × 6 × 6. The structure of the unit cell was optimized (relaxed) before calculation of the electronic properties by varying the volume and positions of ions until each component of stress or force tensors acting on the ions became <10 meV/Å.

Results and Discussion. The optimized unit cell of ReS_2 (Fig. 1) included four formula units, belonged to the triclinic system, and was a pinacoidal (centrosymmetric) unit cell with space group $P\bar{1}$. The occupied Wyckoff position 2*i* corresponded for all ions to two Re ions and four S ions with nonequivalent positions. This suggested that the electrophysical properties of the compound upon its doping depended strongly not only on the properties of the dopant but also on its position in the crystal lattice. Tables 1 and 2 list the lattice constants and positions of ions that were obtained during optimization of the structure and were used for subsequent calculations.

The obtained lattice constants and angles showed good agreement between theory and experiment. Lattice constants *b* and *c* were slightly lower than the experimental values (by 0.6 and 0.8%). This was characteristic of the local density approximation, which usually overestimates interatomic bond strengths. This effect was compensated in the direction perpendicular to the plane of ion packing by van der Waals interactions, which reduced the error by greater than an order of magnitude (to 0.06%) so that it could be said to be comparable to experimental uncertainty.

An analysis of the positions of nonequivalent ions showed that the tendencies observed for the unit-cell parameters persisted. The coordinates of ions along the direction of the van der Waals interaction deviated less than in other directions. The relative deviations for ions were greater than for the lattice parameters. This was explained by compression of the unit cell during modeling and led to an increase of the coordinates of ions to preserve the interatomic bond lengths.

It is noteworthy that the structural properties of low-symmetry crystals are difficult to study because of the many degrees of freedom in such systems. Thus, the potential energy surface had many closely spaced minima corresponding to various configurations of lattice parameters and positions of ions in it. The completeness of the basis set and density of the grid of *k*-points and numerical integration grid also affected the result.

Figure 2 shows the band structure of ReS_2. The bandgap calculated for ReS_2 was $E_g^{\text{calc}} = 1.26$ eV, which agreed well with the usually accepted value $E_g \approx 1.4$ eV. The E_g value characterized the so-called optical bandgap, which included exciton effects and was determined from the experimental study of the optical properties. However, the E_g^{calc} value obtained from density functional theory characterized the so-called electronic bandgap, which did not include exciton effects and should be comparable with results from photoelectron spectroscopy with angular resolution.

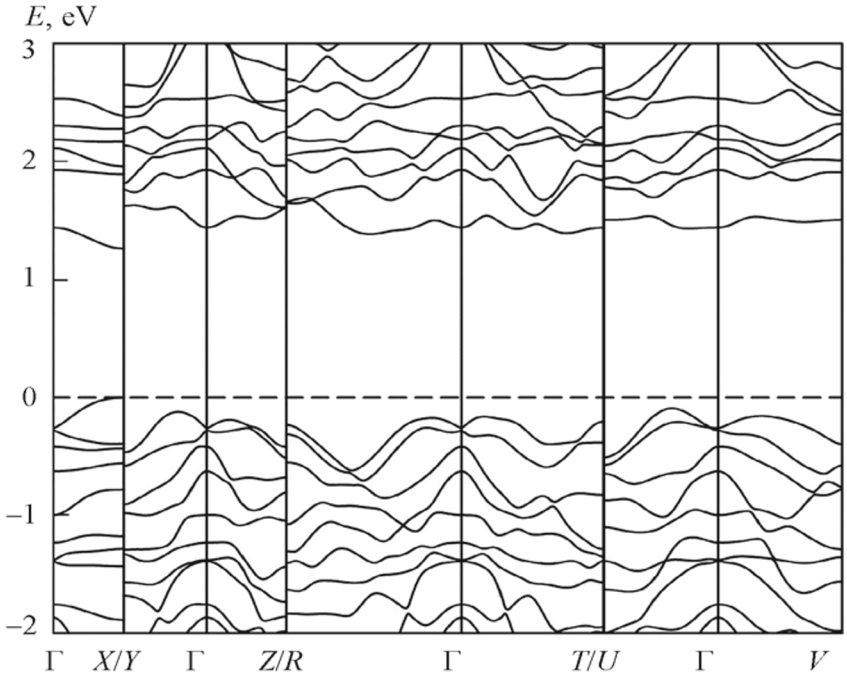

Fig. 2. Band structure of ReS_2 (top of valence band taken as zero).

TABLE 1. Main Parameters of ReS_2 Crystal Structure

Parameter	Calculation	Experiment [13]
a, Å	6.4217	6.4179(4)
b, Å	6.4695	6.510(4)
c, Å	6.4077	6.461(4)
α, deg	121.47	121.10(4)
β, deg	88.17	88.38(5)
γ, deg	106.43	106.47(5)
V, Å^3	215.6	219.3(2)
ρ, g/cm^3	7.71	7.58

Many bands of width 0.2–0.3 eV with distinct dispersion were observed in the valence band along the points of high symmetry. The first direct transition was situated at point *X*, which agreed with the spectroscopic observations. The dispersion of the bands from special positions of high symmetry, except for point *X*, along the direction toward the center of the Brillouin band was jagged and asymmetric with many local minima situated 100–150 meV lower than the top of the valence band. In turn, the conductance band was formed by a smaller number of narrower bands of width 0.1–0.2 eV, local minima of which were 120–150 meV higher than the bottom of the conductance band. This complicated multi-valley band structure was due to the low symmetry of the ReS_2 unit cell. The electrophysical and optical properties of ReS_2 could be expected to be anisotropic and sensitive to mechanical deformations of the crystal because of the many valleys, especially in a two-dimensional state. This could find applications in various items of optoelectronics and sensing.

Figure 3 shows the orbital-projected density of electronic states allowed by type of ion. The valence band was formed by the 5*d*- and 3*p*-states of Re and S ions with a small preference for S. The contributions of S 3*s*-states and Re 5*s*-, 5*p*-, and 6*s*-states were extremely small and independent of energy in the studied range.

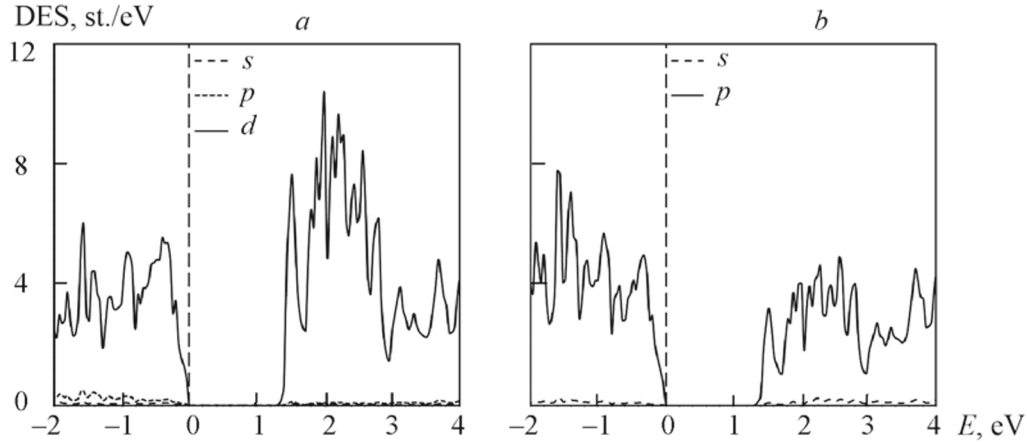

Fig. 3. Density of electronic states for Re (a) and S atoms (b); top of valence band taken as zero.

TABLE 2. Coordinates of Nonequivalent Positions of Ions in ReS_2 Crystal

Ion		*x*	*y*	*z*
Re(1)	Calculation Experiment [13]	0.492212 0.4925(1)	0.057644 0.0564(1)	0.2468* 0.2477(1)
Re(2)	Calculation Experiment [13]	0.502240 0.5026(1)	0.512596 0.5112(1)	0.297617 0.2974(1)
S(1)	Calculation Experiment [13]	0.210800 0.2174(10)	0.249221 0.2498(10)	0.366907 0.3676(9)
S(2)	Calculation Experiment [13]	0.277110 0.2769(9)	0.774641 0.7705(9)	0.382673 0.3819(8)
S(3)	Calculation Experiment [13]	0.759943 0.7562(9)	0.279459 0.2729(9)	0.118646 0.1178(8)
S(4)	Calculation Experiment [13]	0.695960 0.6975(9)	0.754064 0.7526(9)	0.118558 0.1169(9)

Conclusions. The crystal structure and electronic properties of ReS_2 of the triclinic system were investigated by *ab initio* methods in a local density approximation. The structural parameters obtained from numerical modeling agreed with the experimental data. This enabled the use of the local density approximation to be recommended for studying the structural properties of layered Re dichalcogenides in the three- and two-dimensional states and their solid solutions and heterostructures based on Re dichalcogenides with other layered materials. The experimentally direct-band character of bulk ReS_2 was shown to be related to interband electronic transitions at point *X*. The calculated bandgap of 1.26 eV agreed well with the experimental value of ~1.4 eV. Many closely spaced valleys in the band structure suggested the electrophysical and optical properties were anisotropic, The valence and conductance bands were formed by Re-ion 5*d*-states and S-ion 3*p*-states. The effects of other electronic states were insignificant. The density of Re-ion 5*d*-states increased on going from the valence to conductance band while the density of S-ion 3*p*-states decreased. Such an electronic structure was due to the low symmetry of the unit cell with many nonequivalent ions. This suggested that the chemical and physical properties of ReS_2 depended on not only the type of dopant if present but also its position in the crystal lattice. The results were interesting for interpreting and analyzing the experimental data for the chemical, optical, and electrophysical properties of this material and for evaluating and analyzing the properties of heterostructures based on ReS_2.

REFERENCES

1. M. A. Lukowski, A. S. Daniel, F. Meng, A. Forticaux, L. Li, and S. Jin, *J. Am. Chem. Soc.*, **135**, No. 28, 10274–10277 (2013).
2. D. Voiry, M. Salehi, R. Silva, T. Fujita, M. Chen, T. Asefa, V. B. Shenoy, G. Eda, and M. Chhowalla, *Nano Lett.*, **13**, No. 12, 6222–6227 (2013).
3. K. Chang and W. Chen, *ACS Nano*, **5**, No. 6, 4720–4728 (2011).
4. D. J. Late, R. V. Kanawade, P. K. Kannan, and C. S. Rout, *Sens. Lett.*, **14**, No. 12, 1249–1254 (2016).
5. F. Wu, H. Tian, Y. Shen, Z. Hou, J. Ren, G. Gou, Y. Sun, Y. Yang, and T.-L. Ren, *Nature*, **603**, 259–264 (2022).
6. X. Xu, H. Zhao, R. Wang, Z. Zhang, X. Dong, J. Pan, J. Hu, and H. Zeng, *Nano Energy*, **48**, 337–344 (2013).
7. Y. Zhou, E. Song, J. Zhou, J. Lin, R. Ma, Y. Wang, W. Qiu, R. Shen, K. Suenaga, Q. Liu, J. Wang, Z. Liu, and J. Liu, *ACS Nano*, **12**, No. 5, 4486–4493 (2018).
8. J. Gao, L. Li, J. Tan, H. Sun, B. Li, J. C. Idrobo, C. V. Singh, T.-M. Lu, and N. Koratkar, *Nano Lett.*, **16**, No. 6, 3780–3787 (2016).
9. F. Liu, S. Zheng, X. He, A. Chaturvedi, J. He, W. L. Chow, T. R. Mion, X. Wang, J. Zhou, Q. Fu, H. J. Fan, B. K. Tay, L. Song, R.-H. He, C. Kloc, P. M. Ajayan, and Z. Liu, *Adv. Funct. Mater.*, **26**, 1169–1177 (2016).
10. E. Liu, M. Long, J. Zeng, W. Luo, Y. Wang, Y. Pan, W. Zhou, B. Wang, W. Hu, Z. Ni, Y. You, X. Zhang, S. Qin, Y. Shi, K. Watanabe, T. Taniguchi, H. Yuan, H. Y. Hwang, Y. Cui, F. Miao, and D. Xing, *Adv. Funct. Mater.*, **26**, 1938–1944 (2016).
11. C. M. Corbet, C. McClellan, A. Rai, S. S. Sonde, E. Tutuc, and S. K. Banerjee, *ACS Nano*, **9**, No. 1, 363–370 (2015).
12. M. Z. Rahman, K. Davey, and S.-Z. Qiao, *Adv. Funct. Mater.*, **27**, Article ID 1606129 (1–21) (2017).
13. H. H. Murray, S. P. Kelty, R. R. Chianelli, and C. S. Day, *Inorg. Chem.*, **33**, No. **19**, 4418–4420 (1994).
14. R. Coehoorn, C. Haas, J. Dijkstra, and C. J. F. Flipse, *Phys. Rev. B: Condens. Matter Mater. Phys.*, **35**, No. 12, 6195–6202 (1987).
15. W. J. Schutte, J. L. De Boer, and F. Jellinek, *J. Solid State Chem.*, **70**, No. 2, 207–209 (1987).
16. T. Ozaki, *Phys. Rev. B: Condens. Matter Mater. Phys.*, **67**, No. 15, Article ID 155108 (1–5) (2003),
17. T. Ozaki and H. Kino, *Phys. Rev. B: Condens. Matter Mater. Phys.*, **69**, No. 19, Article ID 195113 (1–19) (2004).
18. T. Ozaki and H. Kino, *Phys. Rev. B: Condens. Matter Mater. Phys.*, **72**, No. 4, Article ID 045121 (1–8) (2005).
19. D. M. Ceperley and B. J. Alder, *Phys. Rev. Lett.*, **45**, No. 7, Article ID 566 (1–4) (1980).
20. S. S. Coutinho, M. S. Tavares, C. A. Barboza, N. F. Frazao, E. Moreira, and D. L. Azevedo, *J. Phys. Chem. Solids*, **111**, 25–33 (2017).
21. L. Feng, Z. Wang, and Z. Liu, *Solid State Commun.*, **187**, 43–47 (2014).